

---

Chapter IV  
Magnetic properties

---

## SECTION - A : MAGNETIC HYSTERESIS

### 4.1 INTRODUCTION

Snoek, Gorter and Goodenough [1,2,3] showed that in order to obtain large range of saturation magnetization a variety of substitutional ferrites can be prepared. To prepare ferrites with the desired properties, it is necessary to know their magnetic as well as electrical characteristics. Magnetic properties include saturation magnetization ( $M_s$ ), Neel temperature ( $T_N$ ), susceptibility ( $X$ ) and coercive force ( $H_c$ ) etc. With the help of hysteresis studies one can determine the saturation magnetization, remanance ratio and coercive force. The ferrite with low  $H_c$  are called as 'soft ferrites'. Soft ferrite have high electrical resistivity and low eddy current losses. Soft magnetic materials have been reviewed by Lee and Lynch [4]. The soft ferrites are used in microwave devices, high frequency cores, antennas, transformer cores etc. Ferrites with high  $H_c$  are called as 'hard ferrites'. These are used in loudspeakers, telephones, electronic motors and permanent magnets for which high remanance is desirable [5]. Ferrites with square hysteresis loop characteristics are widely used as memory devices in computers wherein small hysteresis losses are essential

requirements [6]. According to Neel [7] the coercive force is related with saturation magnetization, internal stresses, porosity [8] and anisotropy [9].

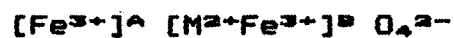
The hysteresis technique is useful to understand the basic magnetic behaviour of solids. The porosity, grain size and stoichiometry have been especially important in controlling the magnetic properties of ferrites. With the help of modern hysteresis measurement techniques it is possible to make visible the real shape of hysteresis on the oscilloscope screen to observe the effect of composition and temperature on it.

#### 4.2 MAGNETIZATION IN FERRITES

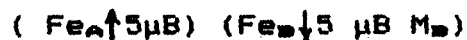
The most fundamental property of ferrites is the magnetization. The magnetization results from the distribution and alignment of magnetic ions on the octahedral and tetrahedral cation sites. If the magnetic atoms are sufficiently close to each other spontaneous magnetization ( $M_s$ ) occurs even in the absence of external field. The electrons can undergo an exchange interaction between neighbouring magnetic ions. This may be direct or may take place via an intermediate non-magnetic ion like oxygen [10]. The

exchange interaction may be either positive or negative and it is based on parallel and antiparallel alignment of the spins of neighbouring atoms respectively. When the exchange interaction is positive it is ferromagnetic and when it is negative then it is either antiferromagnetism or ferrimagnetism depending upon the complete or incomplete cancellation of magnetic moment within the crystal.

The saturation magnetization ( $M_s$ ) in ferrites is calculated from cation distribution. The normal spinels are generally nonmagnetic while inverse spinels are ferrimagnetic. For the ferrites with the inverse spinel structure, cation distribution is expressed as



The  $\text{Fe}^{3+}$  ions on the A site are coupled with their spins antiparallel to those  $\text{Fe}^{3+}$  ions on B site, so that the net moment is due to  $\text{M}^{2+}$  metallic ions.



In case of partially inverted ferrites, some fraction of divalent metal ions are on B sites and the arrangement of moments becomes



and the difference between magnetic moments of A site and B site gives the net magnetic moment

$$\mu_B = M(1-2\delta) - 10(1-\delta)$$

For normal spinel  $\delta = 0$  and for inverse spinel  $\delta = 1$ .

#### 4.3 MAGNETOSTRICTION

The magnetostrictive energy is the magnetostriction parameter and is given by

$$E = \frac{3}{2} \lambda_s \sigma \quad \dots \quad 4.1$$

where,

$\lambda_s$  - saturation magnetization

$\sigma$  - applied stress

Here the energy should be minimized to give the domain freedom of motion. The phenomenon of change in physical dimensions of magnetized material is known as the magnetostriction and is related to the thermal anomalies shown by ferromagnetic substances around Curie point. For cubic materials, the change in dimensions are isotropic i.e only the change in volume take place. But for hexaferrites both changes in volume and shape are observed. This change occur even when the material is cubic. The magnetostriction is closely related to crystal anisotropy and direction of magnetization.

#### 4.4 MAGNETOCRYSTALLINE ANISOTROPY ENERGY

The difference in energy between a state where the magnetization is aligned along an easy direction and state where it is aligned along a hard direction is called "Magnetocrystalline anisotropy energy". It is also the energy needed to rotate the vector from the easy direction to another direction.

For cubic materials, the anisotropy energy can be expressed as

$$E_A = K_1[a_1^2 a_2^2 + a_2^2 a_3^2 + a_3^2 a_1^2] + K_2[a_1^2 a_2^2 a_3^2] + \dots \quad 4.2$$

where  $K_1$  and  $K_2$  are the anisotropy constants which are dependent upon temperature and the material used. These constants determine the direction where  $E_A$  is minimum and  $a_1$ ,  $a_2$ ,  $a_3$  are direction cosines. Anisotropy energy plays an important role in magnetic susceptibility, permeability, magnetostriction and hysteresis phenomena. Magnetic anisotropy may also arise due to stress and shape and it varies with crystal structure and kinds of magnetic ions involved.

#### 4.5 SHAPE OF HYSTERESIS LOOP AND DOMAIN STATE

Following Bean's [11] work the hysteresis loops of micro-powders can be classified in four types namely -

- 1) Multi-domain (MD)
- 2) Superparamagnetic (SP)
- 3) Single-domain (SD-VA)
- 4) Single-domain (SD-CA)

The salient features of the research work carried out in the field are

(1) Loop shapes are independent of the parameters of the intensity of magnetization and magnetocrystalline anisotropy constant ( $K_1$ ).

(2) SD and SP shapes are temperature dependent, where as MD shapes are temperature independent.

(3) Experimentally determined shapes agree with the theoretically computed shapes for SD and SP cases while for MD cases it is not so.

The general shape of curve is shown in Figure - 4.1. At the beginning the material is in the demagnetization state i.e at point 'O'. On the application of magnetic field, the magnetization increases until the saturation value is reached, this is shown by the curve OABC. This part of the curve is called the magnetization curve. Then by reducing the magnetic field to zero, increasing it in the reverse direction, decreasing to zero and then increasing it to the original value the curve CDEFGC results. The curve

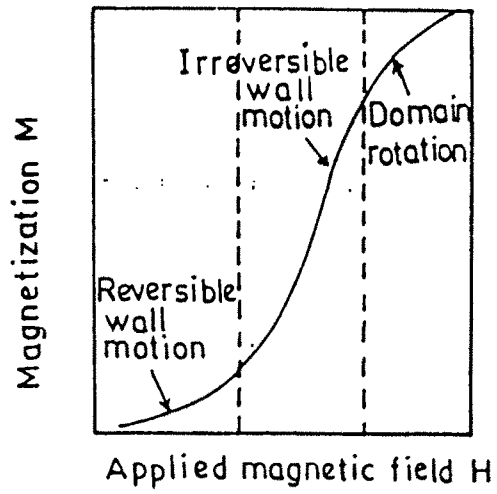


Fig. 4·A·1(a) — A TYPICAL MAGNETIZATION CURVE .

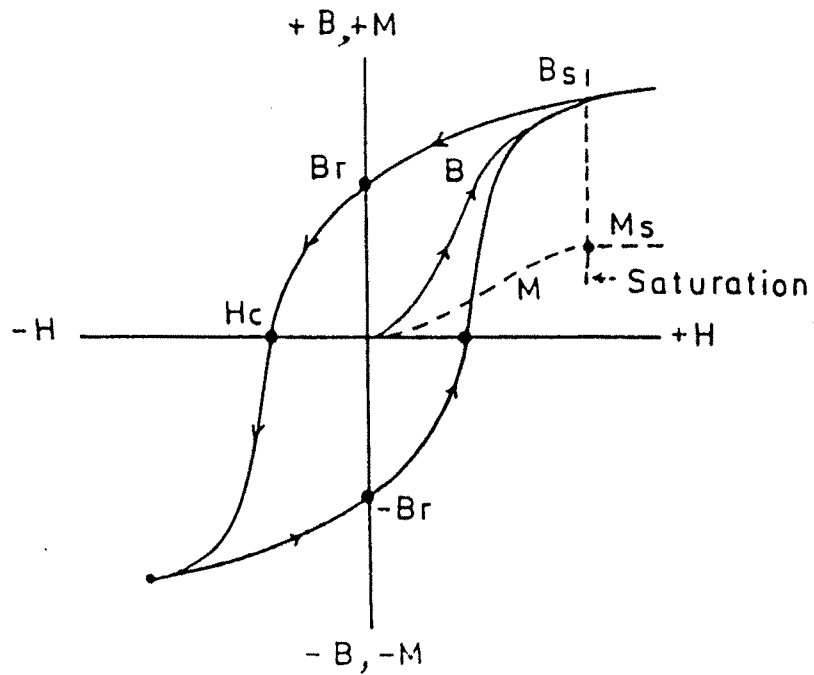


Fig. 4·A·1(b) — GENERAL FEATURES OF HYSTERESIS LOOP.



is known as Hysteresis curve and is symmetric in nature.

In the Hysteresis curve the reversible wall displacements take place in the initial part. In the central part of the curve the irreversible wall displacements and Berkhausen jumps take place. On reducing the field the domains relax to the nearest easy direction of magnetization because of anisotropy forces. On reversing the field, some boundary movements followed by a Berkhausen jump take place. Towards the bottom of the curve, rotations predominate again and the saturation is reached in the reversed direction.

#### 4.6 CALCULATION OF $M_s$ AND $nB$

The vertical displacement on oscilloscope were taken for Ni sample of mass 0.2679 gm. As the standard magnetization for Ni sample is 53.35 emu/gm and applied field is 3 K Gauss, the total magnetization of Ni sample is

$$53.35 \times 0.2679 = 14.289 \text{ emu}$$

The vertical divisions on CRO are 17 and hence the calibration factor (c.f.) is

$$\text{c.f.} = \frac{\text{Total magnetization of Ni sample}}{\text{divisions for Ni sample}}$$

$$\text{c.f.} = \frac{14.289}{17} = 0.8405 \text{ emu/div}$$

The vertical reading for the samples were taken at room temperature. By using these readings the magnetization of the samples was calculated with the help of following relations -

$$\sigma_s = \text{Reading for the pellet} \times \text{c.f. (emu)}$$

hence  $\sigma_s$  is emu/gm .

$$\sigma'_s = \frac{\sigma_s}{\text{mass of pellet}} \quad (\text{emu/gm})$$

$$M_s = (1 - p) dx \times \sigma'_s \quad \dots \quad 4.3$$

$$\text{where } p = \text{porosity} = \frac{dx - d_a}{dx} \times 100$$

$$dx = \text{x-ray density} = \frac{8 \times \text{Mol. wt. of sample}}{N a^3}$$

$N$  = Avogadros number

$a$  = Lattice constant

$$d_a = \text{actual density} = \frac{\text{mass of pellet}}{\text{volume}}$$

$$= \frac{\text{mass of pellet}}{\pi r^2 t}$$

where  $t$  = thickness of the pellet,  $r$  = radius of the pellet

The magnetic moment per formula unit in Bohr magnetons (nB) is given by

$$nB = \frac{\text{Mol. wt.} \times \sigma's}{5585} \dots 4.4$$

#### 4.7 EXPERIMENTAL TECHNIQUES

The essential parts of the hysteresis loop tracer [12] are -

1. Electromagnet
2. Pick-up coil system
3. Balancing and Integrating network and
4. Pre-amplifier.

The circuit diagram of the apparatus is shown in Figure 4.2.

1. Electromagnet: The two C cores (English Electric Company, type WR/110/32/13) of laminated grain-oriented silicon steel with cross-section of the poles  $5 \times 2.5 \text{ cm}^2$  have been used for this purpose. From one of C cores, a piece of 1.2 cm in thickness was cut out to get a pole gap of 1.2 cm. The two C cores were joined together. The energizing coil for the magnet consists of 2200 turns of 20 swg super enamelled copper wire (Resistance 11.5 ohms) wound on a perspex former and firmly held together on a wooden base.

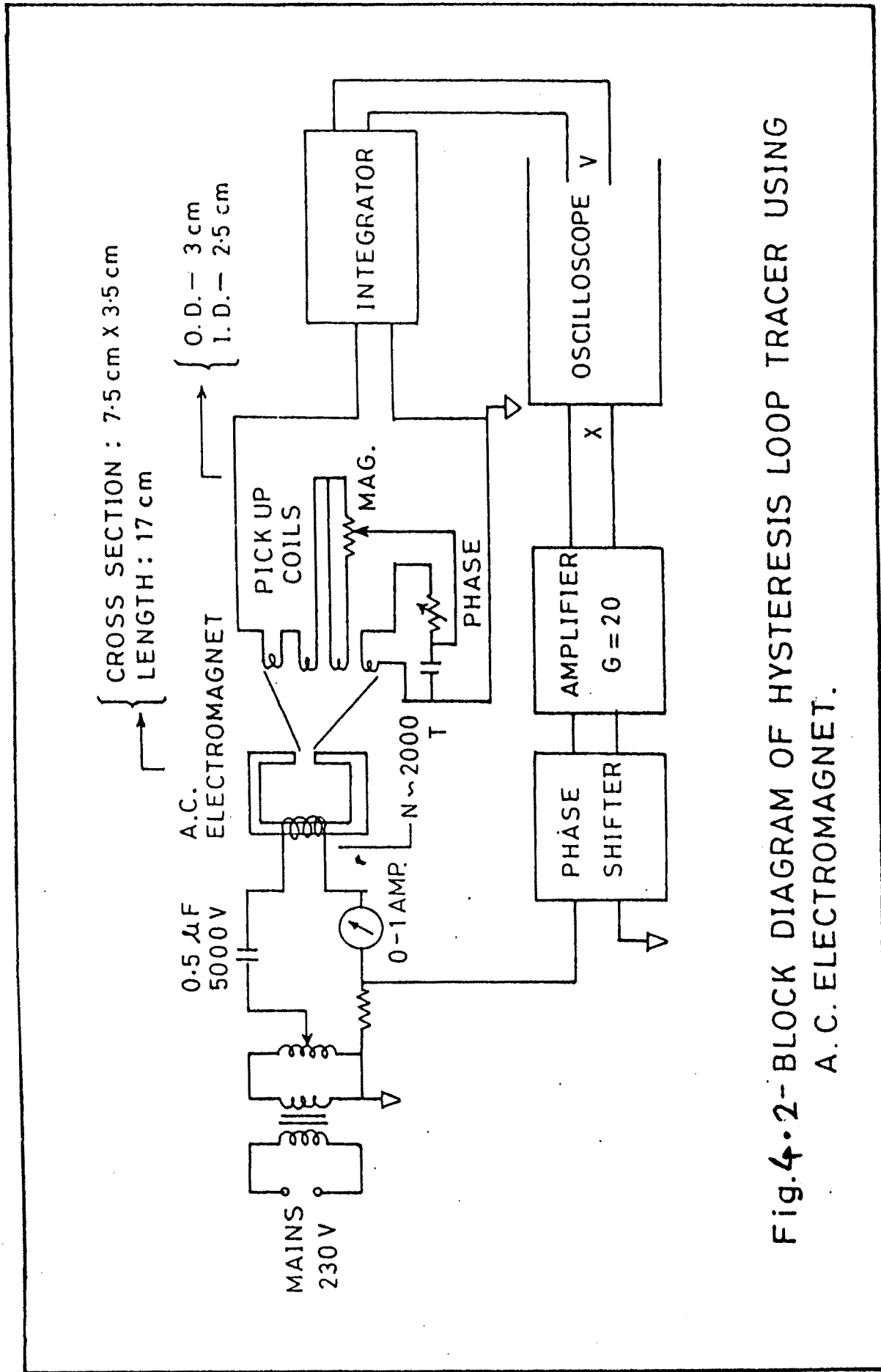


Fig. 4.2- BLOCK DIAGRAM OF HYSTERESIS LOOP TRACER USING A.C. ELECTROMAGNET.

2. Pick-up coil system: A multi coil, which can be introduced in the pole gap, serves as a pick-up coil system. It consisted of four different windings, one over the other, wound with 39 swg super enamelled copper wire on a perspex former. The multi-coil is connected through the balancing and integrating network to a amplifier and then to the Y - plates of the oscilloscope. The input of the X - plates is taken from the emf developed across a resistance connected in series with the energizing coil. A phase shifting network with proper inductance and variable resistance is also provided as shown in Figure 4.2.

The multi-coil unit was slid into the pole gap and the current in the energizing coil was increased to produce the required field. The potentiometer and variable resistance in the balancing network were then adjusted to get a horizontal trace on the oscilloscope. After reducing the current to zero, the multi-coil was pulled out and the ferrite pellet kept at the central gap in the multi-coil spool to be introduced into the pole gap. The current in energizing coil was raised to a sufficient value till the sample saturates. The hysteresis loop produced on the oscilloscope was recorded for an accurate measurement of magnetization.

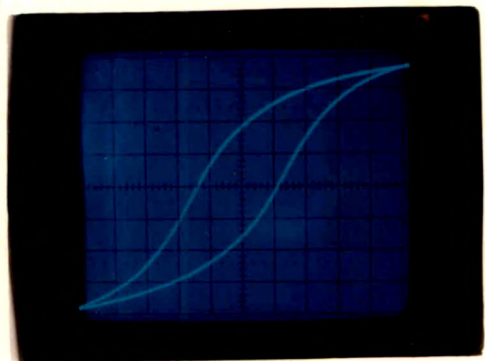
Pure nickel (99.9%) in the form of cylindrical pellet ( $M_s = 53.35$  emu/g) at  $27^\circ\text{C}$  was used for calibration of y-axis. The horizontal scale was calibrated by measuring the field, the pole gap with a sensitive Gauss meter while d.c. were passed through the energizing coil. For obtaining hysteresis loops a.c. fields are used and hence, the necessary corrections for d.c. fields were incorporated.

#### 4.8 RESULTS AND DISCUSSION

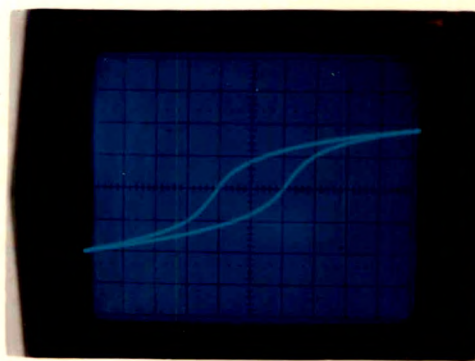
Hysteresis loops for nickel and  $\text{Zn}_x\text{Mg}_{1-x}\text{Ti}_t\text{Fe}_{2-2t}\text{O}_4$  (where  $x = 0.3$ ,  $t = 0, 0.05, 0.1, 0.2$  and  $x = 0.05, 0.2, 0.3, 0.4, 0.6$ ) ferrite samples at room temperature are presented in Figures 4.3 and 4.4. From the hysteresis data, the values of  $M_r/M_s$  and magnetic moment (nB) were calculated at room temperature for all the samples. The data is presented in Tables 4.1 and 4.2.

From Table 4.1 it is seen that

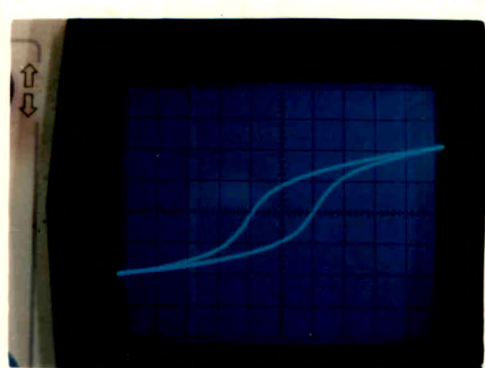
- (1) the value of nB increases on addition of zinc and reaches maximum at  $x = 0.4$ . The samples became non-magnetic for  $x > \text{or} = 0.6$ .
- (2) the values of  $M_r/M_s$  (squareness ratio) decrease monotonically on the addition of zinc in the system.



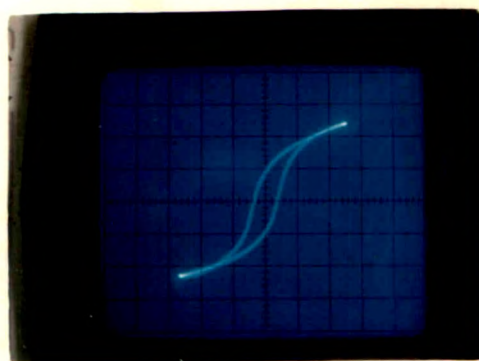
$t=0$



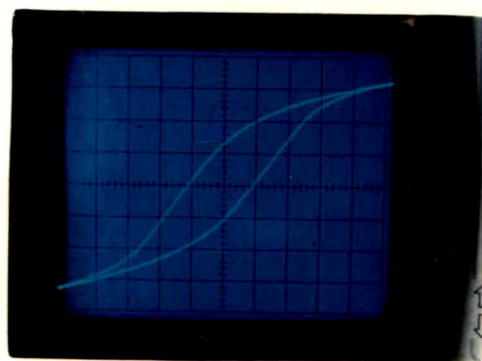
$t=0.05$



$t=0.1$

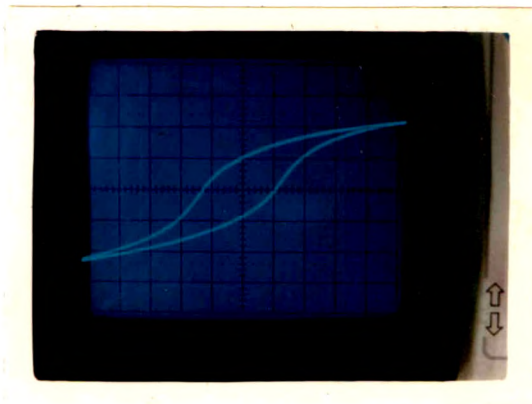


$t=0.2$

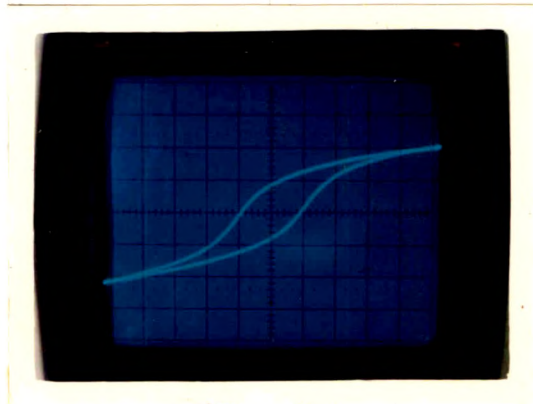


Ni-Sample

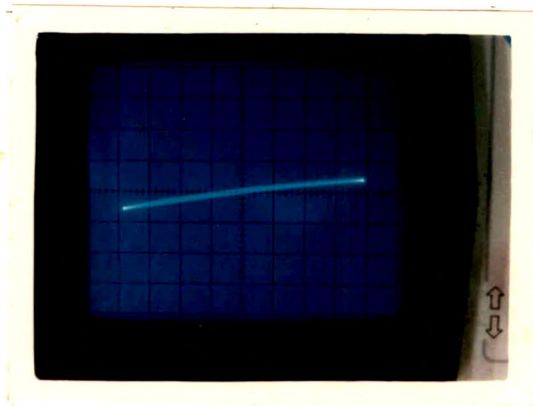
Fig: 4:3.- Hysteresis loops for  $Zn_xMg_{1-x}Ti_tFe_{2-2t}O_4$   
( $x=0.3$ ) ferrite samples:



$$X = 0.2$$



$$X = 0.4$$



$$X = 0.6$$

Fig. 4:4-Hysteresis loops for  $Zn_xMy_{1-x}tTi_tFe_{2-2t}O_4$   
( $t=0.05$ ) ferrite samples.



Table 4.1

Data for Bohr magnetons nB and Mr/Ms for  $Zn_xMg_{1-x}Ti_0.05Fe_{2-2x}O_4$  ferrites,  $t = 0.05$

x	nB, Bohr Magnetons	Mr/Ms
0.2	2.10	0.36
0.3	2.14	0.35
0.4	2.18	0.30
0.6	-	-

Table 4.2


Data for Bohr magnetons nB and Mr/Ms for  $Zn_xMg_{1-x}Ti_0.05Fe_{2-2x}O_4$  ferrites ( $x = 0.3$ )

t	nB, Bohr Magnetons	Mr/Ms
0.0	2.16	0.28
0.05	2.14	0.35
0.1	1.56	0.35
0.2	1.05	0.32

The values of magnetic moment were obtained by using the relation 4.4 [13].

In Table 4.2 variation of  $n_B$  with the content of  $Ti^{4+}$  is shown. It is seen that the magneton number decreases on the addition of  $Ti^{4+}$ . On the basis of existing predictions [14-16] the preferred sites for Zn is A and that for Ti, Sn and Ni is B. The number of workers have postulated movement of ions to the non-preferred sites i.e.  $Ti^{4+}$  to B sites [14],  $Sn^{4+}$  to A sites [15] and  $Zn^{2+}$  to B sites [16]. The magnetization, lattice parameter variation studies on titanium, zirconium and tin substituted nickel zinc ferrites have been carried out by Das et al [17] and they conclude that when added in small amount  $Ti^{4+}$  occupies A sites.

For the series  $Zn_xMg_{1-x+t}Ti_tFe_{2-2t}O_4$  (where  $t = 0, 0.05, 0.1, 0.2$  and  $x = 0.3$  the values of Bohr magneton numbers decrease due to the reduction of A-B interaction. It is known that substitution of  $Zn^{2+}$  in Mg ferrite results in triangular type of spin arrangement. Thus the variation of  $n_B$  with the content of zinc is as per the Y-K theory. The substitution of  $Ti^{4+}$  results in over all decrease of  $Fe^{3+}$  ions which leads to decrease of  $n_B$ . However, substitution of  $Ti^{4+}$  can also cause additional canting.



According to the Neel's model the Curie temperature for the series of ferrites is proportional to the product of the iron ( $\text{Fe}^{3+}$ ) contents on the <sup>200</sup> sites and their inter sub lattice distances and angles. In the present series the  $\text{Ti}^{4+}$  ions change the iron ion concentration from 2 to  $2-2t$ . Therefore the number of ferrous ions decreases on the octahedral sites. Thus reduction in  $\text{Fe}^{3+}$  ions both on octahedral and tetrahedral sites leads to the reduction of Curie temperature.

Fomenko et al [18] have studied the effect of replacing iron with titanium, zirconium and hafnium on the initial permeability of Mn-Zn ferrites. They found that crystalline dimensions do not change on the addition of  $\text{Ti}^{4+}$  in the system. The values of  $M_r/M_s$  did not change significantly on addition of  $\text{Ti}^{4+}$  in the present system. This property is exhibited due to MD type of particles present in the system.

## SECTION B - A.C. SUSCEPTIBILITY STUDIES

### 4.8 INTRODUCTION

A polycrystalline ferrite may contain

- (1) Multi-domain (MD)
- (2) Single-domain (SD) and

(3) Superparamagnetic (SP) particles depending upon its thermal history. A.C. susceptibility and magnetization studies explore the domain state of particles.

The susceptibility is defined as the ratio of the magnetization (M) produced in the substance to the applied magnetic field (H)

$$K = M/H \text{ emu/cm}^3 \text{ Oe} \quad \dots \quad 4.6$$

since M is the magnetic moment per cm<sup>3</sup>, K is called volume susceptibility. The mass susceptibility (X) is defined as  $X = K/\rho$  emu/g Oe ... 4.7

The shapes of  $X_{ac}$ -T curves have been correlated with the domain structure by Radhakrishnanmurthy et al [19]. In the  $X_{ac}$ -T curves the Curie temperatures have been estimated at which  $X_{ac}$  drops to zero. Many workers have used  $X_{ac}$ -T curves to interpret domain state in the ferrites [20,21].

Magnetic grains, which have a few hundred angstrom, dimension are termed as single domain(SD) for which magnetization direction is fixed in space. The very small grains, up to about hundred angstrom size are called as superparamagnetic (SP). When the thermal energy of SD particles becomes comparable to effective magnetic anisotropy energy, the

magnetization fluctuates in the two long easy axes of the particle and the grain is said to exhibit superparamagnetism (SP). Hence the magnetic states of SD and SP are interchangeable by temperature. The temperature is referred to as the blocking temperature ( $T_b$ ), which is less than the Curie temperature ( $T_c$ ) of the concerned material. The volume ( $v$ ), the saturation magnetization ( $M_s$ ) and coercive field ( $H_c$ ) are related by the relation given by Neel(22) as

$$V M_s H_c = 2 k T_b \dots\dots\dots 4.6$$

where  $k$  is Boltzmann constant.

#### 4.9 EXPERIMENTAL TECHNIQUES

To measure the a.c. susceptibility, the apparatus developed by Likhite et al [13] was used. The circuit diagram of the same is shown in Figure 4.5. The apparatus essentially consists of a Helmholtz coil, two pick-up coils, a furnace and a sample holder. Two coils made of 100 turns of enamelled copper wire with the mean diameter of 18.4 cm called as Helmholtz coils were fixed one over the other separated by a distance equal to their mean radii. One of the coil produces magnetic field of 7 Oe operating at 263 Hz and another coil produces a emf directly proportional to the

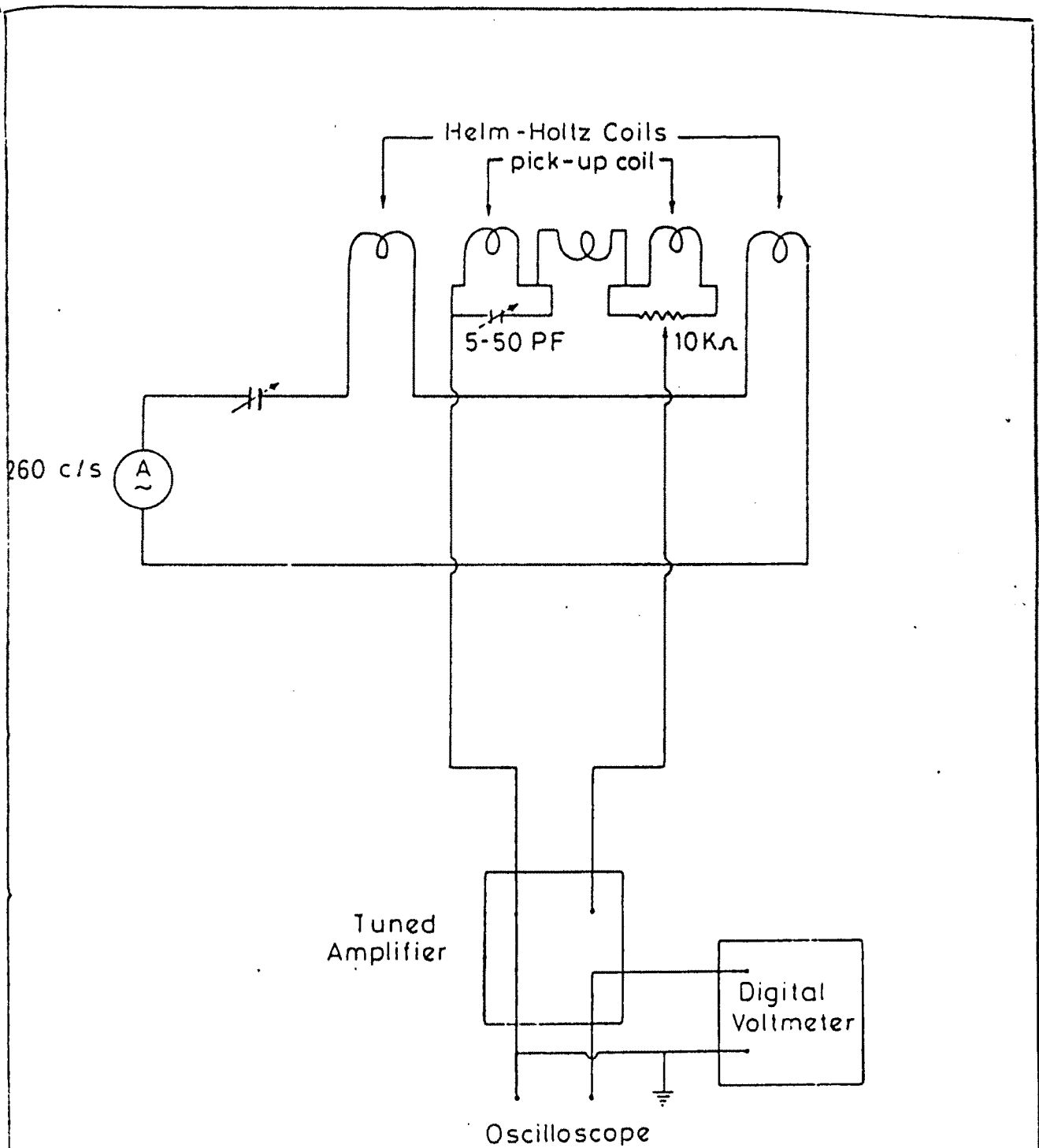


Fig. 4.5 Schematic diagram of initial susceptibility apparatus.

susceptibility of magnetic material at different temperature ( $X_T$ ) and at room temperature ( $X_{RT}$ ). The measured emf ( $X_T$ ) is related to real susceptibility ( $X$ ) by the relation

$$X_T = \frac{X}{(1 + NX)} \quad \dots \quad 4.9$$

where,  $N$  is the demagnetization factor.

The measurement of normalized a.c. susceptibility ( $X_T/X_{RT}$ ) of the samples as a function of temperature was carried out in powder form. A sample kept at the center of balanced double coil which itself is at the center of Helmholtz coil system producing an alternating magnetic field behaves like an alternating dipole and induces a differential emf in the double coil. The current to the Helmholtz coil was supplied by an oscillator and a high quality power amplifier. The signal induced in the double coil is rectified and read on a digital voltmeter (DVM). The digital voltmeter was calibrated in terms of magnetic moments. The temperature of the furnace was maintained by a power supply and it was measured by using a platinum rhodium thermocouple. The measurements were taken from room temperature to 500 °C. The glass jacket containing the sample was removed slightly out of the heating

arrangement to record the background effect. The magnetic moments were observed for different constant temperatures.

#### 4.10 RESULTS AND DISCUSSION

High temperature a.c. susceptibility measurements were first carried out on iron by Hopkinson [23] who showed that it reached a peak value just before  $T_c$  and became zero rapidly. Applying this technique, Radhakrishnamurthy et al [24] have explored the complex magnetic behaviour of titanomagnetites. Ferrites have been studied by this method by many workers [25-28]. Three types of peaks have been reported in  $\chi_{ac}$ -T curves as shown in Figure 4.6.

1. Hopkinson peak is the one occurring just before the  $T_c$  if any magnetic material in the MD state.

2. Isotropic peak, which could be seen clearly for a magnetic material in the MD form and only if the material has a temperature at which the magnetocrystalline anisotropy is zero.

3. SD peak which could be obtained only if the sample under investigation has a substantial proportion on SD particles in it and occurs at the  $T_b$  of the



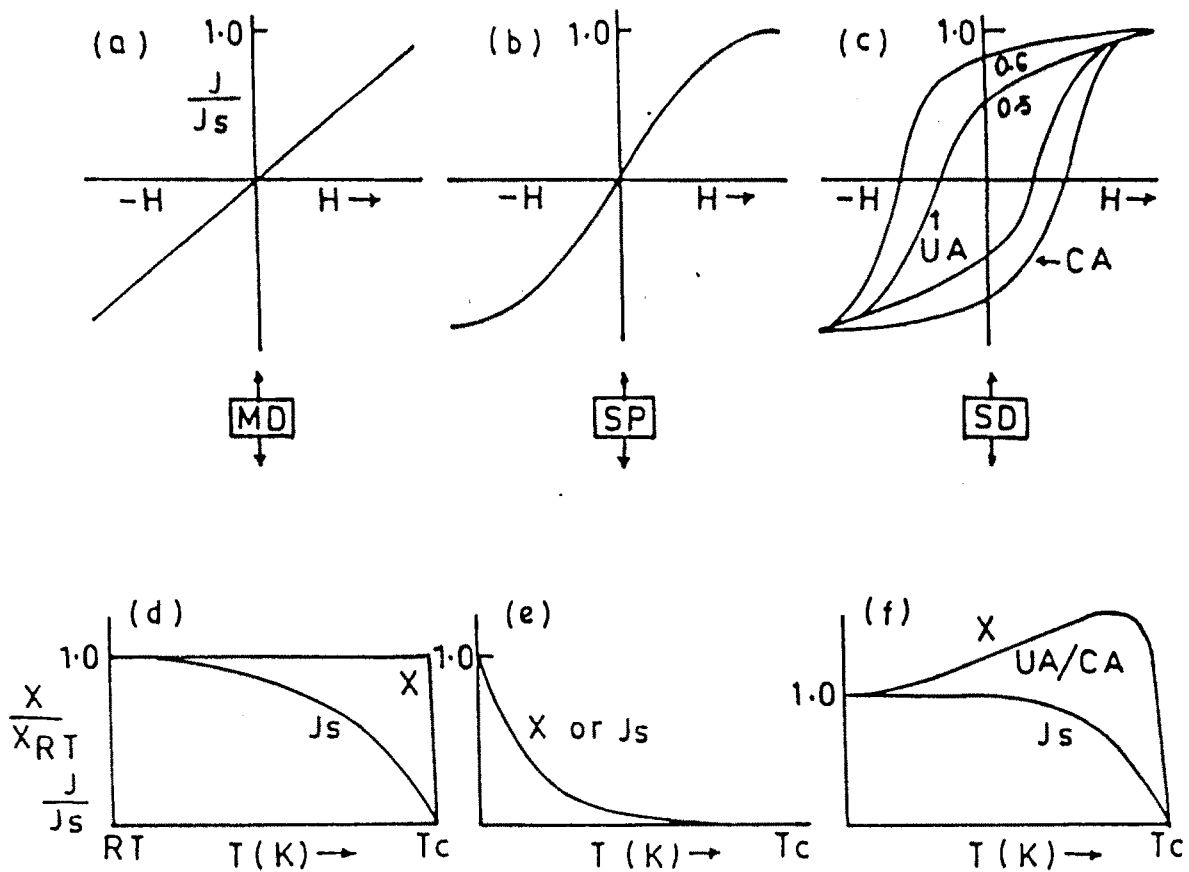


Fig. 4.6 Schematic hysteresis loops normalized  $x$ - $T$  and  $J_s$ - $T$  curves for samples containing grains in different domain states, MD-multidomain SP-superparamagnetic and SD-optimum single-domain states. In (c) UA denotes dominant uniaxial anisotropy and CA dominant crystalline anisotropy. Interesting point to be noted is that the  $x$ - $T$  and  $J_s$ - $T$  curves may be similar for a sample consisting of sufficiently fine SP particles.

particles. If  $T_b$  is mid-way between  $T_A$  and  $T_c$  solid line curves results.

$X_{ac}$  in case of SP particles shows a continuous decrease with the increase of temperature and become zero at  $T_c$ . The shapes of  $X_{ac}$ -T curve inform about the domain state of a particular sample as long as mixtures of several domain states are not involved.

Applying the concepts discussed above and observations made, the following conclusions have been drawn.

In Figure 4.7 temperature variation of normalized susceptibility for the samples  $Zn_xMg_{1-x+t}Ti_tFe_{2-2t}O_4$  where  $x = 0.3$ ,  $t = 0, 0.05, 0.1, 0.2$  has been shown. The following observations could be made -

1.  $X/X_{RT}$  does not vary with the temperature up to the Curie point.
2. For  $Zn_{0.3}Mg_{0.7}Fe_2O_4$  ferrite,  $X_{ac}$ -T curve shows a sharp peak.
3. Near the Curie temperature there is decrease of  $X/X_{RT}$  which indicates the single phase material.
4. If the content of  $Ti^{4+}$  is increased, the peak vanishes and there is a gradual decrease of  $X/X_{RT}$ .

Thus, it can be interpreted that  $Zn_{0.3}Mg_{0.7}Fe_2O_4$  contains the SD grains. While with the substitution of

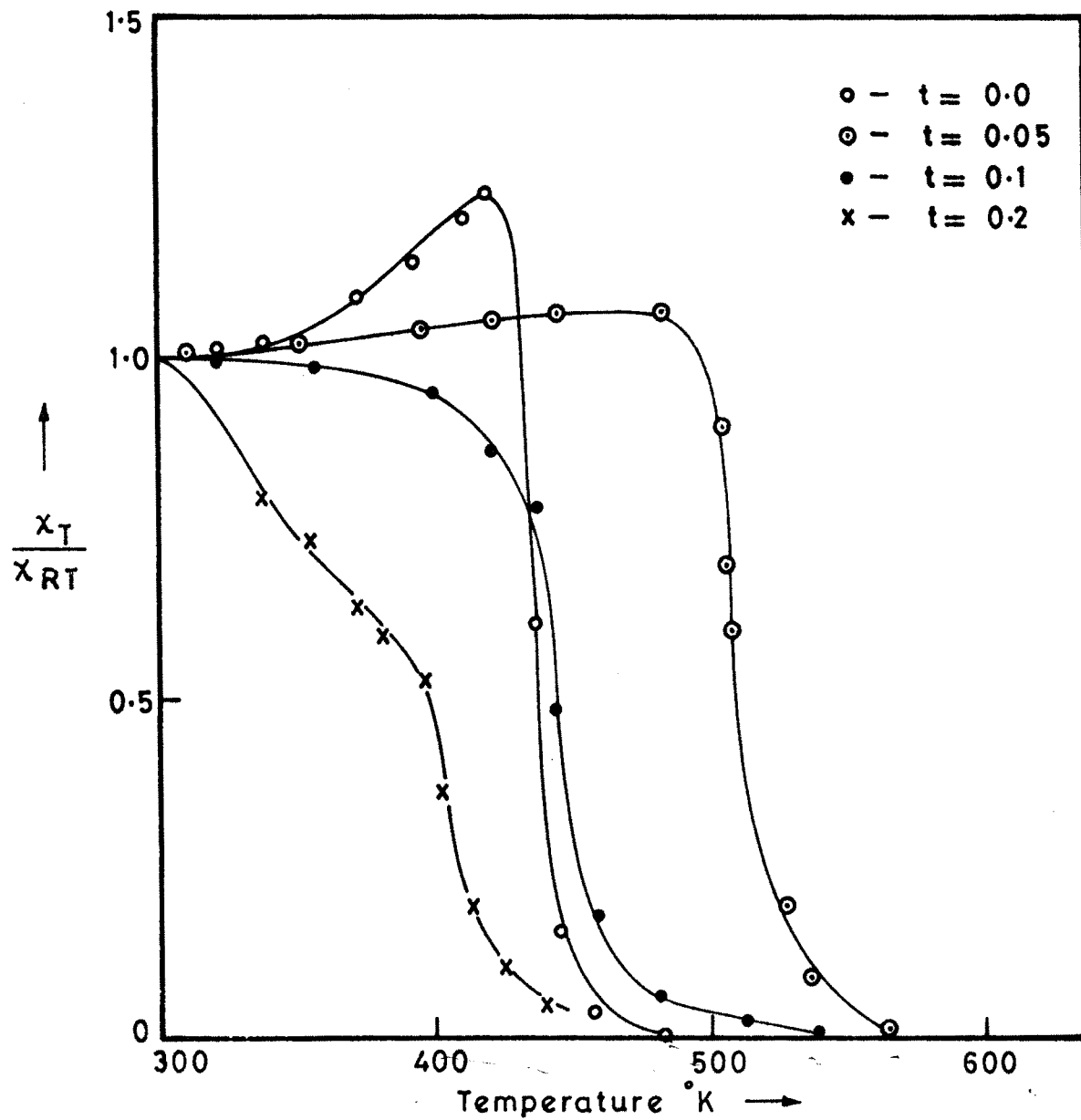


FIG. 4.7- VARIATION OF SUSCEPTIBILITY WITH TEMPERATURE FOR  $Zn_xMg_{1-x+t}Ti_tFe_{2-2t}O_4$ . (where  $x = 0.3$ )

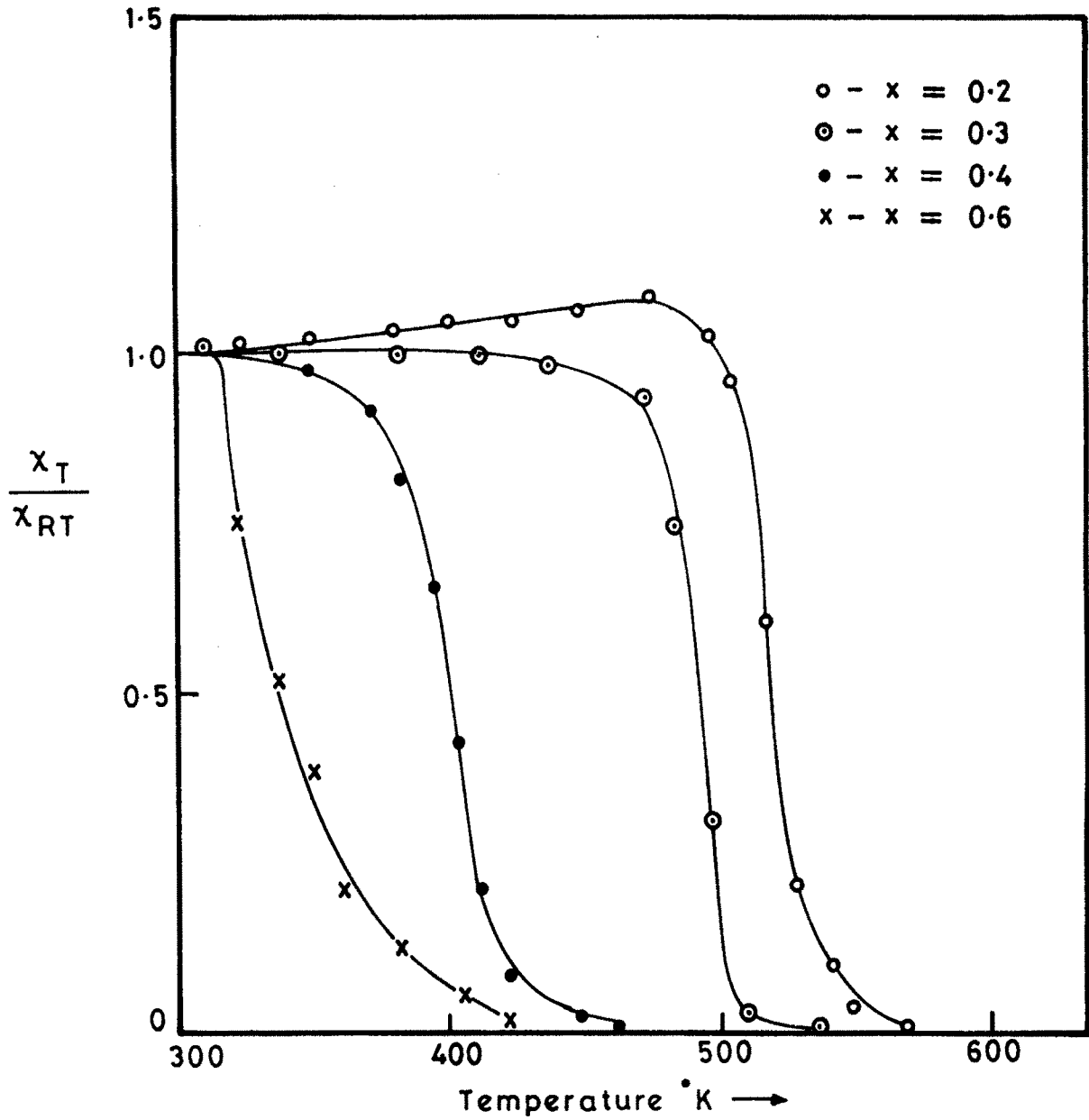


FIG. 4.8 - VARIATION OF SUSCEPTIBILITY WITH TEMPERATURE FOR  $Zn_xMg_{1-x+t}Ti_tFe_{2-2t}O_4$ . (where  $t=0.05$ )

Ti<sup>4+</sup> transition to MD state occurs. The nature of a.c. susceptibility variation with temperature suggests that MD type of particles are present in the samples.

In Figure 4.8 the variation of  $\chi_{ac}-T$  for the samples  $Zn_xMg_{1-x+t}Ti_tFe_{2-2t}O_4$  where  $t = 0.05$ ,  $x = 0.2, 0.3, 0.4, 0.6$  has been shown. Following conclusion have been made from it.

1. The sharp peaks do not appear in  $\chi_T/\chi_{dT} - T$  variation at any temperature.

2. Broad peaking tendency is exhibited by the composition for  $t = 0.05$  and  $x = 0.2$ .

3. The Curie temperature decreases with the addition of zinc in the system.

Thus from above it can be concluded that addition of Ti<sup>4+</sup> in small amount favours (SD) type of particles in MgFe<sub>2</sub>O<sub>4</sub>. Addition of Zn<sup>2+</sup> tends to decrease the peak height in  $\chi_{ac}-T$  variation which suggests that presence of Zn<sup>2+</sup> inhibits the formation of (SD) particles. Thus the addition of zinc forces the samples to go from (SD) to (SD and MD) state [28]. The Curie temperature  $T_c$  decreases on addition of zinc due to the reduction of A-B interaction. The non-linear fall of Curie temperature suggests that canted spins are favoured.

## SECTION C - INITIAL PERMEABILITY

### 4.11 INTRODUCTION

Permeability is a useful property for deciding the various applications of ferrite. In radio frequency region the requirement is large permeability with low losses in the frequency range of interest. The initial permeability ( $\mu_i$ ) is structure sensitive property which depends upon the method of preparation, porosity and grain size [29,30]. When magnetic material is subjected to an a.c. field it produces rapid movement of magnetic domains walls and since permeability is related to the movement of these walls, it gets affected. Rado and Terris [31] have observed low-frequency dispersion in ferrites which they have attributed to domain wall displacements. The absence of low frequency resonance indicated the absence of domain wall movements. The hindrance to the domain wall motion results in low values of  $\mu_i$ .

A demagnetized magnetic material is divided in a number of Weiss domains, separated by Bloch walls. In the Weiss domains all magnetic moments are oriented parallel to each other and its saturation magnetization has value  $M_s$ . In the Weiss domain walls there is gradual change of magnetization direction from one

direction to the next. The walls are bound to equilibrium position. These positions result from the integrations with the magnetization in the neighbouring domains and from the influence of pores, crystal boundaries and chemical inhomogeneities which tend to favour certain wall positions.

Initial permeability arise from two main mechanisms [32]. They are

- (1) Contribution from spin rotation and
- (2) Contribution from domain wall motion.

But the contribution from spin rotation is smaller than that of domain wall motion [33]. The permeability due to domain wall motion is given by the relation

$$(\mu_i - 1) = 3\pi M_s^2 D / 4\gamma \quad \dots \quad 4.10$$

where,

$M_s$  - saturation magnetization

$D$  - mean grain diameter

$\gamma$  - magnetic domain wall energy.

The initial permeability  $\mu_i$  increases with temperature up to Curie temperature. This is due to anisotropy field usually decreases with the temperature much faster than the  $M_s$ . The variation of  $\mu_i$  with crystal anisotropy  $K_1$  is shown in Figure 4.9. It passes through zero at the temperature  $T_k$  and the permeability

rises to a high peak at this point. Sometimes  $\mu$ -T curve exhibit double peak feature due to presence of excessive ferrous ions within the material.

#### 4.12 EXPERIMENTAL TECHNIQUES

Variation of initial permeability with temperature was determined by using LCR bridge ( APLAB Model Autocompute Q-4910). The samples in the form of toroids were made with the help of die having inner diameter of 1 cm and outer diameter of 1.5 cm. An insulated copper wire was wound on the toroid so as to form a core. The values of inductance and Q-factor were noted with increasing temperature for the fixed frequency of 1 KHz. The readings were noted from room temperature to 500 °C.

The initial permeability was calculated by using the relation

$$L = 0.0046 N^2 \cdot \mu_i \cdot h \times \log_{10} (d_1/d_2) \dots 4.11$$

where L is the inductance in microhenries, h is the thickness of the core in inches,  $d_1$  and  $d_2$  are outer and inner diameters in inches,  $\mu_i$  is the permeability of the core and N is the number of turns.



#### 4.13 RESULTS AND DISCUSSION

Variation of initial permeability ( $\mu_i$ ) with temperature is shown in Figures 4.10 and 4.11. From Figure 4.10 it is seen that when  $Ti^{4+}$  is added in small quantities permeability  $\mu_i$  increases at all temperatures. From the nature of the graph it is observed that for the ferrite  $Zn_{0.3}Mg_{0.7}Fe_2O_4$  as the temperature increases the permeability gradually increases, reaches a peak and drops sharply with the further increase of temperature. The sharp decrease of  $\mu_i$  indicates single phase formation of the material. In a sample with  $t = 0$ , a peak is observed in  $\mu_i$ -T variation.

Globus [32] has given the following relation for the initial permeability  $\mu_i = Ms^2 dm/K_1$  where  $dm$  is the mean grain diameter,  $K_1$  is magnetocrystalline anisotropy constant and  $Ms$  is the magnetization. The initial permeability arises due to spherical bulging of the domain walls under an applied magnetic field Fomenko and Bakshina [18] have studied the effects of replacing iron with titanium, zirconium and hafnium on the Mg-Zn ferrite. They have found that  $\mu_i$  increases on addition of  $Ti^{4+}$  and  $Hf^{4+}$ .

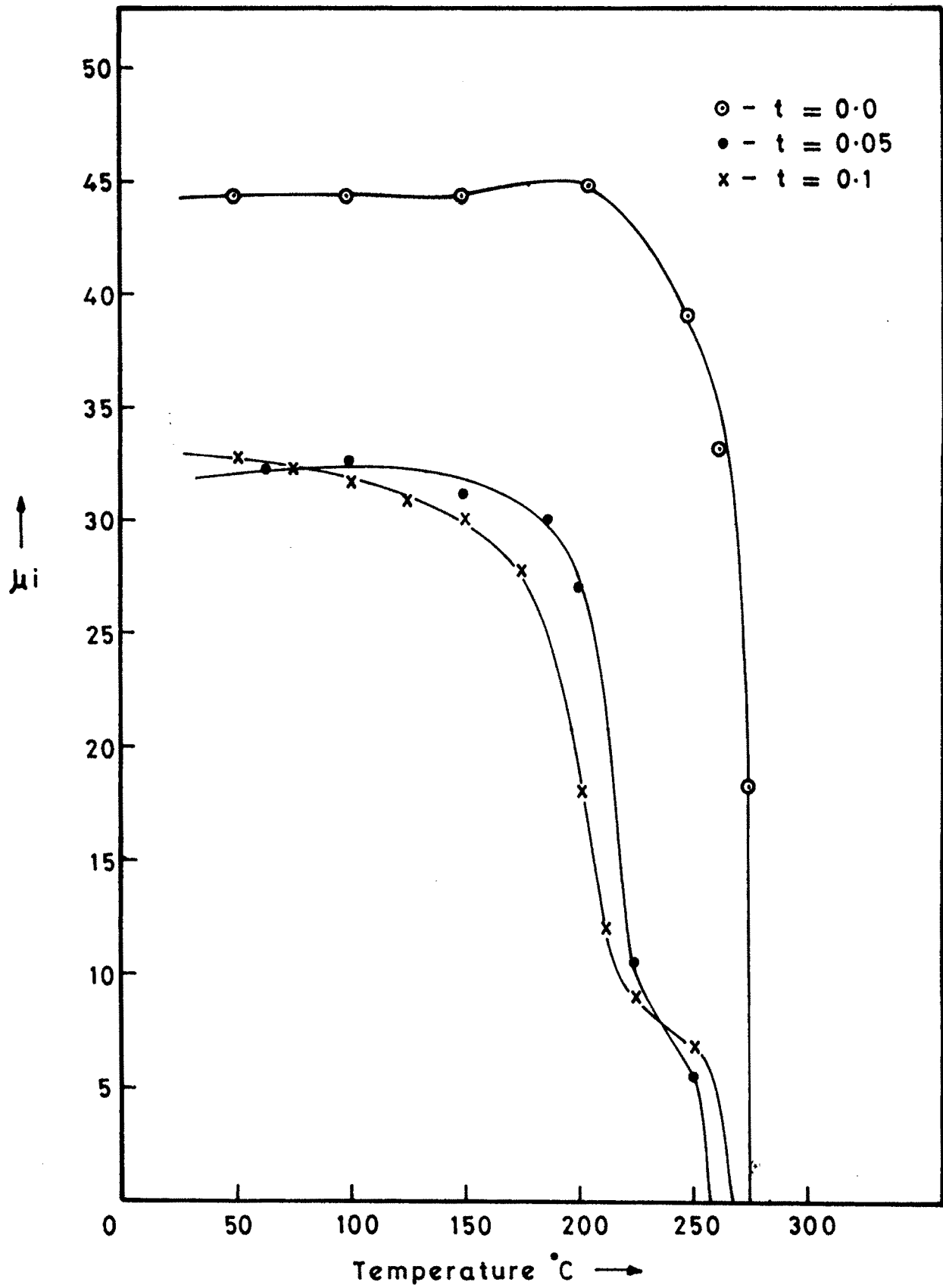


FIG. 4.10 VARIATION OF INITIAL PERMEABILITY WITH TEMPERATURE FOR  $Zn_xMg_{1-x+t}Ti_tFe_{2-2t}O_4$ . (where  $x = 0.3$ )

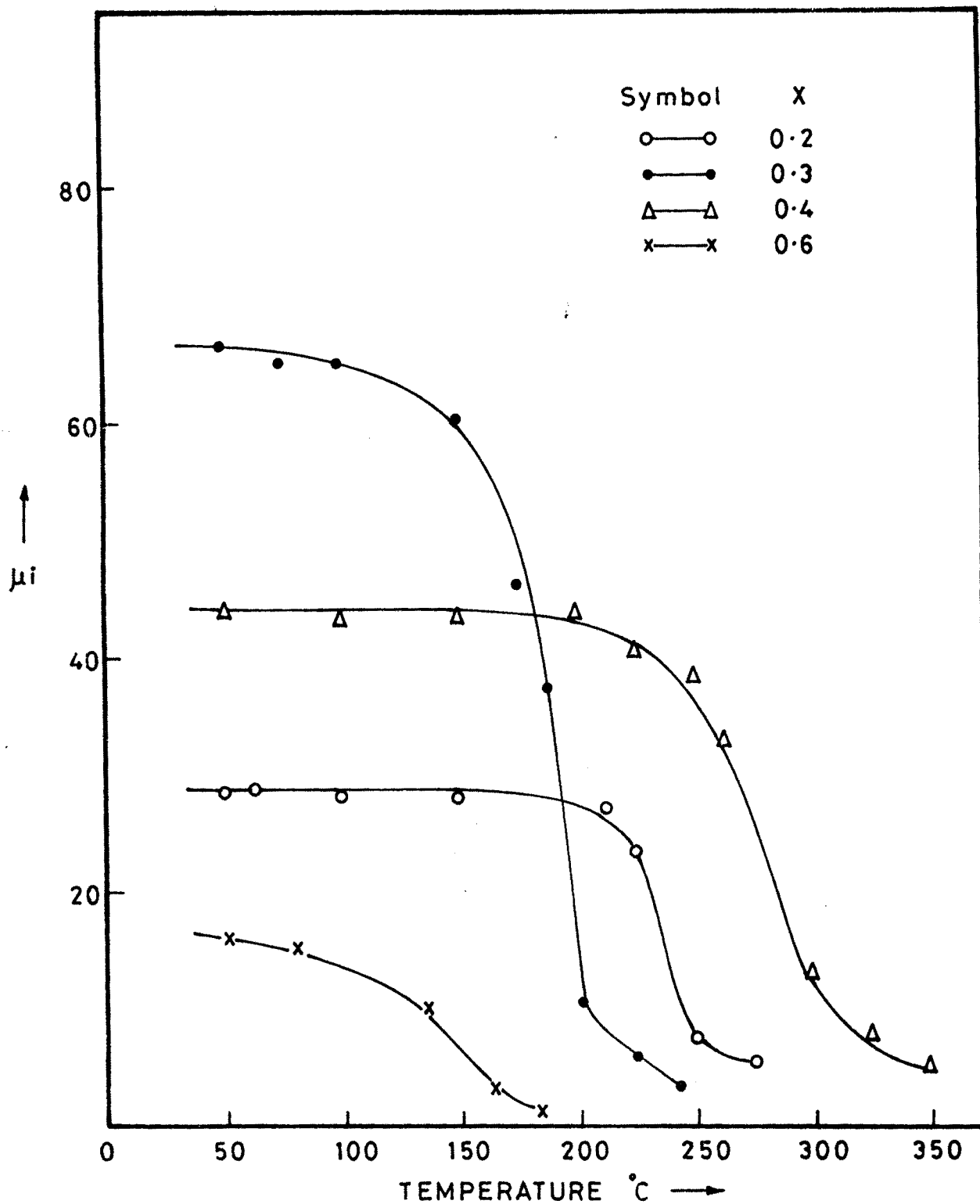


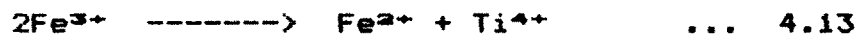
FIG. VARIATION OF INITIAL PERMEABILITY WITH TEMPERATURE FOR  $Zn_xMg_{1-x+t}Ti_tFe_{2-2t}O_4$  (where  $t=0.05$ ).

According to Wijn et al [34] the initial permeability of polycrystalline spinel is given by

$$\mu_i - 1/2\pi = M_s^2/K_1 \quad \dots \quad 4.12$$

where  $M_s$  is the saturation magnetization and  $K_1$  is the anisotropy constant. According to the above equation the initial permeability is proportional to the square of saturation magnetization hence the saturation magnetization mainly affects the initial permeability. The above equation is used to calculate  $K_1$  from the observed values of  $M_s$  and  $\mu_i$  at room temperature. The values of  $K_1$  with the composition are noted in Tables 4.3 and 4.4. From these tables it is seen that for series  $Zn_xMg_{1-x+t}Ti_{0.05}Fe_{1-t}O_4$  the  $K_1$  decreases with the increases of Zn and decrease of Mg.

Titanium is a tetravalent ion and it can cause localization of  $Fe^{2+}$  ions according to this equation.



The increase in  $\mu_i$  may be due to positive contribution by  $K_1$  to the total anisotropy constant which appears when  $Fe^{3+}$  ions are converted to  $Fe^{2+}$ .

Temperature variation of  $\mu_i$  in case of  $Zn_xMg_{1-x+t}Ti_tFe_{2-2+t}O_4$  where  $t = 0.05$  and  $x = 0.2, 0.3, 0.4, 0.6$  and  $x = 0.3$  and  $t = 0, 0.05, 0.1, 0.2$  can be explained as follows. In most magnetic

materials  $\mu_i$  increases with temperature up to the Curie temperature  $T_c$ . This is because of anisotropy field usually decreases with temperature much faster than  $M_s$ . The crystal anisotropy  $K_1$ , as shown in the Figure 4.9, passes through zero as the temperature  $T_k$  and the permeability then rises to a high peak at this point. It is observed that near  $T_c$  permeability drops sharply for both the series which indicates that impurity phases are not present in the material. The Curie temperature decreases with increase of  $Zn^{2+}$  and also Curie temperature decreases with increase amount of  $Ti^{4+}$  concentration. Tables 4.5 and 4.6 show the Curie temperatures obtained from permeability and susceptibility measurements.

The variation of temperature coefficient of  $\mu_i$  [35] is defined as

$$T_F = \frac{\mu_2 - \mu_1}{(T_2 - T_1) \mu_1} \quad \dots 4.14$$

where  $\mu_i$  is the initial permeability at temperature  $T_1$  °K and  $\mu_2$  - is the initial permeability at temperature  $T_2$  °K.

The values of temperature coefficient and composition are noted in Tables 4.3 and 4.4.

The intrinsic parameter of the material that affect initial permeability, saturation magnetization

Table 4.3

Data on anisotropy constant and temperature factor for  $Zn_xMg_{1-x}Ti_2Fe_{2-2x}O_4$  ferrites

t	x	Anisotropy constant $K_1$ , ergs/cm <sup>3</sup>	Temp. Factor $T_F$ , deg C <sup>-1</sup>
0.0		$2.5 \times 10^3$	$6.76 \times 10^{-4}$
0.05	0.3	1.1 "	-
0.1		1.5 "	- 1.46 "
0.2		1.2 "	- 9.79 "

Table 4.4

Data on anisotropy constant and temperature factor for  $Zn_xMg_{1-x}Ti_2Fe_{2-2x}O_4$  ferrites

x	t	Anisotropy constant $K_1$ , ergs/cm <sup>3</sup>	Temp. Factor $T_F$ , deg C <sup>-1</sup>
0.2		$1.8 \times 10^3$	$0.19 \times 10^{-4}$
0.3	0.05	1.1 "	-
0.4		1.0 "	- 6.4 "
0.6		-	- 6.3 "

**Table 4.5**

**Data on Curie temperature from Permeability and susceptibility experiments for  $Zn_xMg_{1-x}Ti_1Fe_{2-2x}O_4$  ferrites**

t	x	Curie temperature °C from	
		Permeability	Susceptibility
0		270	-
0.05	0.3	247	252
0.1		230	177
0.2		-	139

**Table 4.6**

**Data on Curie temperature from Permeability and susceptibility experiments for  $Zn_xMg_{1-x}Ti_1Fe_{2-2x}O_4$  ferrites**

x	t	Curie temperature °C from	
		Permeability	Susceptibility
0.2		275	267
0.3	0.05	240	239
0.4		187	147
0.6		112	77

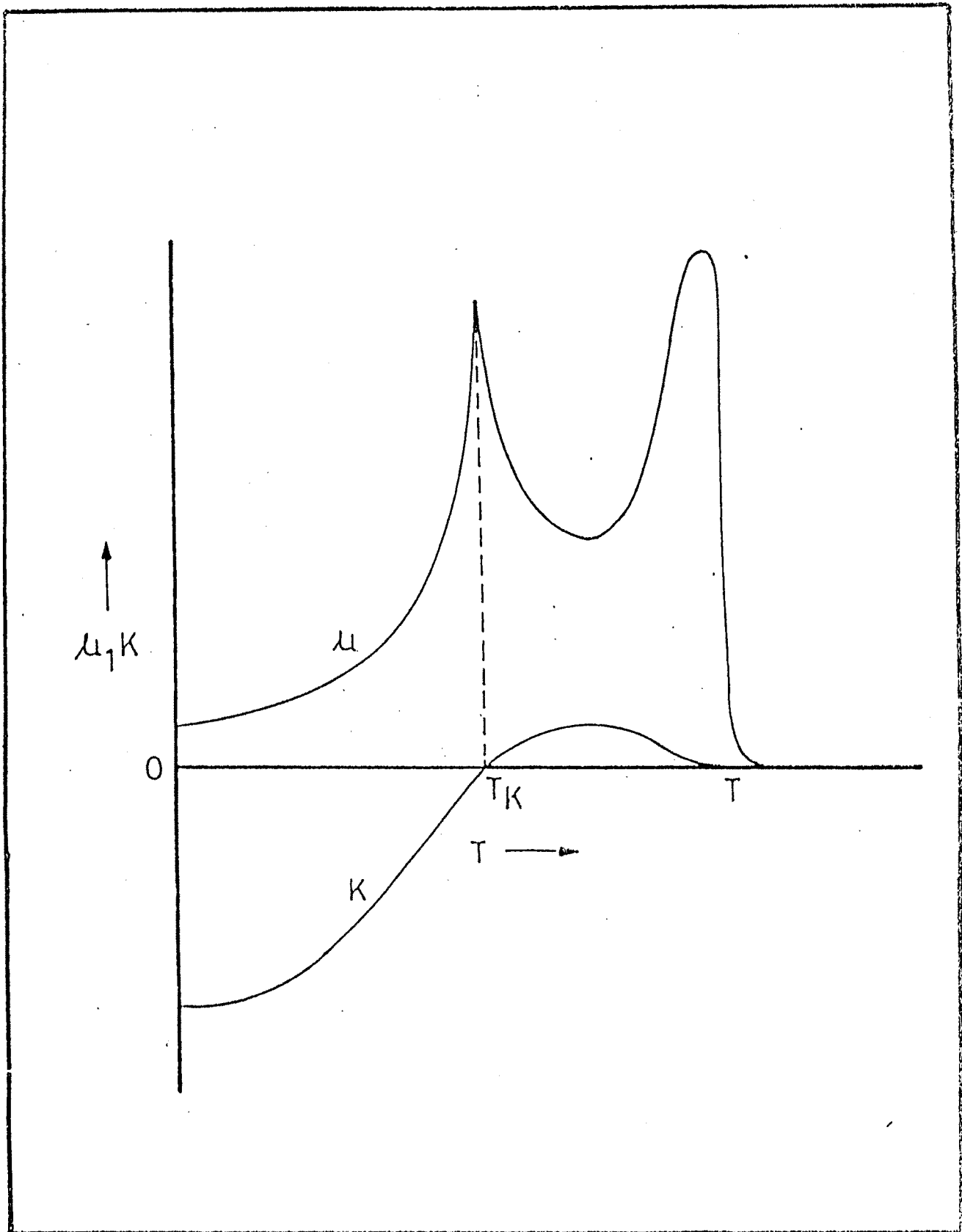


Fig. 4.9



and magnetocrystalline anisotropy. Since both  $M_s$  and  $K_1$  vary with temperature  $\mu_i$  is a complicated function of temperature and it is difficult to derive any qualitative inference. The positive temperature coefficient suggests a increase in  $\mu_i$  while the negative value suggests a decrease in  $\mu_i$  with temperature. It is seen that when the temperature is increased,  $\mu_i$  increases and after a maximum peak near curie temperature  $\mu_i$  drops sharply for further increase of temperature. The sharp decrease of  $\mu_i$  indicates single phase formation of the material.

## REFERENCES

1. Snoek J.L.  
Phillips Tech. Rev. 8 (1946) 353
2. Gorter E.W.  
Philips Res. Repts. 9 (1954) 295
3. Goodenough J.B.  
"Magnetization and Chemical Bond"  
Interscience, London (1962)
4. Lee E.W. and Lynch A.C.  
"Advances in Phys." (1959) 292
5. Richards E.E. and Lynch A.C.  
"Soft Magnetic Materials for Telecommunications",  
Pergamon Press Ltd. London (1953)
6. Hoh S.R.  
"Evaluation of High Performance Core Materials",  
Tele.-Tech. 2 (1953) 86
7. Neel L.  
Properties of magnetic of ferrites,  
ferromagnetism and antiferromagnetism  
Ann. Phys., 3 (1948) 137
8. Srivastav C.M., Patani M.J. and Srinivasan T.T.,  
J. Appl. Phys. 53 (3) (1982) 2107
9. Alper A.M.,  
"High Temperature Oxides",  
Academic Press, N.Y. (1971)
10. Hoselitz K.,  
"Magnetic Properties" in Physical Metallurgy  
Ed. R.W.Cahn. II Revised edition  
North Holland Pub. Co. London (1970) 1233
11. Bean C.P.  
J. Appl. Phys. 26 (1955) 381
12. Likhite S.D., Radhakrishnamurthy C. and  
Sahasrabudhe P.W.  
Ind. Acad. Sci. 87(A) (1978) 245

13. Radhakrishnamurthy C., Likhite S.D. and Sashtri N.P.  
Phil. Mag. 23 (1971) 503
14. Gorter E.W.  
Philips Res. Repts. 9 (1954) 403
15. Puri R.K. and Vershney Usha J.  
Phys. Chem. Solids 44 (1983) 655
16. Blasse G.  
Phillips Res. Repts. 18 (1963) 400
17. Das A.R., Ananthan V.S. and Khan D.C.  
J. Appl. Phys. 57 (1) (1985) 4189
18. Fomenko G.V. and Bashkirov L.A.  
"Chemistry and Technology of Oxides Magnetic Materials" [in Russian] No. IV IZd, Volgogradsk Politekhn Instituta P - 67 (1978)
19. Radhakrishnamurthy C.  
J. Geoglog. Soc. (India) 26 (9), (1985) 640
20. Baldha G.J., Upadhyaya R.V. Kulkarni R.G.  
Mat. Res. Bull. 21 (1986) 1015
21. Kulkarni R.G. and Upadhyay R.V.  
Mater. Lett. 4 (3) (1986) 168
22. Neel L.  
Adv. Phys. 4 (1955) 191
23. Hopkinson J.  
Philips Tras. Roy Soc. (London). AL-80 (1989) 443
24. Radhakrishnamurthy C., Likhite S.D., Deutsch E.R. and Murthy G.S.  
Phys. Earth Planet Inter. 30 (1982) 281
25. Venkatesh Rao & Keer H.V.  
Pramana 19 (1982) 103
26. Stoner E.C. and Wolhfarth E.P  
Philips Trans. of Roy. Soc. A-240 [1948] 599

27. Chougule R.S., Radhakrishnamurthy C. R. K.,  
Sampathkumaram E.V., Malik S.K. and Vijayraghavan.  
Mat. Res. Bull., 18 (1983) 817
28. Jadhav S.R.  
Ph.D Thesis, Shivaji University, Kolhapur (1990)
29. Guillaud C.  
Proc. IEE 104-B, (1957) 165
30. Standley K.J.  
"Oxide Magnetic Materials"  
Clarendon Press Oxford 98 (1972)
31. Rado G.T. and Terris A.  
Phys. Rev. 83 (1951) 177
32. Globus A., Duplex P. and Gayot M.  
IEEE Trans. Magn. (USA) 7 (1971) 617
33. Globus A. and Duplex P.  
J. Appl. Phys. (USA) 39 (1968) 727
34. Wijn H.P.J. and Smit J.  
"Advances In Electronics and Electron Physics"  
( Vol. VI Physical Properties of Ferrites )  
Ed. L Morton, Academic Press Inc. N.Y. (1954)
35. Heck. I.C.  
"Magnetic Materials and their Applications"  
Butterwirths, London, England (1974) 30